Alexandria Engineering Journal (2016) 55, 3037–3052

HOSTED BY

Alexandria University

Alexandria Engineering Journal

www.elsevier.com/locate/aej
www.sciencedirect.com

ORIGINAL ARTICLE

Double-diffusive natural convection in an enclosure filled with nanofluid using ISPH method

Abdelraheem M. Aly [a,*], **Zehba A.S. Raizah** [b]

[a] *Department of Mathematics, Faculty of Science, South Valley University, Qena, Egypt*
[b] *Department of Mathematics, Faculty of Science for Girls, King Khalid University, Abha, Saudi Arabia*

Received 25 October 2015; revised 18 May 2016; accepted 4 June 2016
Available online 31 August 2016

KEYWORDS

Enclosure;
Double-diffusive;
ISPH;
Nanofluid;
Natural convection

Abstract The double-diffusive natural convection in an enclosure filled with nanofluid is studied using ISPH method. The model used for the nanofluid incorporates the effects of Brownian motion and thermophoresis. In addition the thermal energy equations include regular diffusion and cross-diffusion terms. In ISPH algorithm, a semi implicit velocity correction procedure is utilized and the pressure is implicitly evaluated by solving pressure Poisson equation. The results are presented with flow configurations, isotherms, concentration and nanoparticle volume fraction contours and average Nusselt and Sherwood numbers for different cases. The results from this investigation are well validated and have favorable comparisons with previously published results. It is found that, among all cases, a good natural convection can be obtained by considering the double diffusive case. An increase in Soret number accompanied by a decrease in Dufour number results in an increase in average Nusselt number and a decrease in average Sherwood number.

1. Introduction

The term "nanofluid" refers to a liquid containing a suspension of metallic or non-metallic nanometer-sized solid particles and fibers (nanoparticles). The term was suggested by Choi [1]. The characteristic feature of nanofluids is thermal conductivity enhancement, a phenomenon observed by Masuda et al. [2]. This phenomenon suggests the possibility of using nanofluids in a variety of engineering applications, including advanced nuclear systems [3]. The general topic of heat transfer in nanofluids has been surveyed in a review article by [4] and a book by Das et al. [5]. A review of the heat transfer characteristics of nanofluids has been made by Wang and Mujumdar [6]. Rahimi-Gorji et al. [7] introduced an analytical investigation of the heat transfer for the microchannel heat sink (MCHS) cooled by different nanofluids (Cu, Al_2O_3, Ag, TiO_2 in water and ethylene glycol as base fluids). They performed this study by the porous media approach and the Galerkin method and their results are compared with numerical procedure. Pourmehran et al. [8] presented a thermal and flow analysis of a fin shaped microchannel heat sink (MCHS) cooled by different nanofluids (Cu and Al_2O_3 in water) based on "saturated porous medium" and least square method. They calculated the effective thermal conductivity and viscosity of nanofluid by KKL correlation. Central composite design (CCD) is applied to obtain the desirability of the optimum value of the nanofluid flow characteristics. Rahimi-Gorji et al. [9] applied

* Corresponding author.
E-mail address: abdelreheam.abdallah@sci.svu.edu.eg (A.M. Aly).
Peer review under responsibility of Faculty of Engineering, Alexandria University.

http://dx.doi.org/10.1016/j.aej.2016.06.036

Nomenclature

C	concentration of species
D_B	Brownian diffusion coefficient
d_0	particle size
D_T	thermophoresis diffusion coefficient
D_{CT}	Soret diffusivity
D_{TC}	Dufour diffusivity
D_S	solute diffusivity of porous medium
g	gravitational acceleration vector
H	enclosure height
k	thermal conductivity
Le	Lewis number
Ln	nanofluid Lewis number
Nb	Brownian motion parameter
Nd	modified Dufour parameter
Nr	buoyancy ratio parameter
Nt	thermophoresis parameter
Nu	Nusselt number
P	pressure
Pr	Prandtl number
Sr	Soret parameter
Sh	Sherwood number
Ra_T	thermal Rayleigh number
Ra_c	concentration Rayleigh number
T	temperature
t	time
u, v	velocity vectors
U, V	dimensionless velocity components
W	enclosure width
x, y	Cartesian coordinates
X, Y	dimensionless coordinates

Greek symbols

α	thermal diffusivity
β_T	thermal expansion coefficient
β_C	compositional expansion coefficient
μ	viscosity
Φ	dimensionless species concentration
υ	kinematic viscosity
φ	rescaled nanoparticle volume fraction
ϕ	nanoparticle volume fraction
θ	dimensionless temperature
τ	dimensionless time
ρ_f	density of base fluid
ρ_p	nanoparticle mass density
$(\rho c)_f$	heat capacity of the fluid
$(\rho c)_p$	effective heat capacity of the nanoparticle material
∇^2	Laplacian operator

an analytical investigation for unsteady motion of a rigid spherical particle in a quiescent shear-thinning power-law fluid. They used collocation Method (CM) and Numerical Method to solve the present problem. Also, Pourmehran et al. [10] applied an analytical investigation for unsteady flow of a nanofluid squeezing between two parallel plates. Their results were compared with those obtained from Collocation Method (CM), Least Square Method and the established Numerical Method (Fourth order Runge-Kutta) scheme. They calculated the effective thermal conductivity and viscosity of the nanofluid using the Maxwell–Garnett (MG) and Brinkman models, respectively.

Double-diffusive convection refers to buoyancy-driven flows induced by combined temperature and concentration gradients. The cases of cooperating thermal and concentration buoyancy forces where both forces act in the same direction and opposing thermal and concentration buoyancy forces where both forces act in opposite directions have been considered in the literature. Double diffusion occurs in a wide range of scientific fields such as oceanography, astrophysics, geology, biology and chemical processes (Béghein et al. [11]). Ostrach [12] reported complete reviews on the subject. Lee and Hyun [13] and Hyun and Lee [14] have reported numerical solutions for double-diffusive convection in a rectangular enclosure with aiding and opposing temperature and concentration gradients. Their solutions were compared favorably with reported experimental results. Mamou et al. [15] have reported an analytical and numerical study of double diffusive convection in a vertical enclosure.

In recent years, the SPH method had been applied into compressible and incompressible viscous fluid flow problems [16,17]. The SPH was originally developed in compressible flow, and then some special treatment was required to satisfy the incompressible condition. One approach is to run the simulations in the quasi-incompressible limit, that is, by selecting the smallest possible speed of sound which still gives a very low Mach number ensuring density fluctuations [16,17]. This method is known as the weakly compressible smoothed particle hydrodynamics (WCSPH). Cummins and Rudman [18] introduced a new formulation for enforcing incompressibility in Smoothed Particle Hydrodynamics (SPH). The method uses a fractional step with the velocity field integrated forward in time without enforcing incompressibility. The resulting intermediate velocity field is then projected onto a divergence-free space by solving a pressure Poisson equation derived from an approximate pressure projection. Our group improved ISPH method by introducing both velocity divergence condition and relaxing density invariance condition in the source term of pressure Poisson equation (Asai et al. [19]). Aly et al. [20] modeled the surface tension force for free surface flows and an eddy viscosity based on the Smagorinsky subgrid scale model using incompressible smoothed particle hydrodynamics (ISPH) method. They declared that, the eddy viscosity has clear effects in adjusting the splashes and reduces the deformation of free surface in the interaction between two fluids and also, the proposed stabilization using relaxing density invariance with velocity divergence appeared in the source term of pressure Poisson equation has an important role to keep the total volume of fluid by decreasing particles clustering. In addition, Aly et al. [21] applied the stabilized incompressible SPH method to simulate free falling of rigid body and water entry/exit of circular cylinder into water tank. Aly [22] simulated fluid-soil-structure interactions using stabilized ISPH method. In this thesis, the evaluation of pressure is

stabilized by including relaxing density invariance with velocity divergence of pressure Poisson equation and the current improvement try to avoid the particles clustering. In addition, soil erosion by fluid flow during dam break is simulated and discussed in detail using stabilized ISPH method. Aly and Lee [23] adapted ISPH method to simulate impact flows associated with complex free surface. They tested the accuracy and efficiency of the proposed incompressible SPH method using several sample problems with largely distorted free surface, including 2D dam-break over horizontal and inclined planes with different inclination angles, as well as the water entry of a circular cylinder into a tank.

Numerical modeling of transient natural convection by using SPH method has also been investigated. Chaniotis et al. [24] proposed a remeshing algorithm based on weakly compressible flow approach and performed a comprehensive study for non-isothermal flows. SPH simulation of flow and energy transport using SPH was performed by Szewc et al. [25]. In their study, natural convection in a square cavity problem with a Boussinesq and a non-Boussinesq formulation was performed. They introduced a new variant of the Smoothed Particle Hydrodynamics (SPH) simulations of the natural convection phenomena. Danis et al. [26] modeled the transient and laminar natural convection in a square cavity using SPH method with a discretization tool on uniform Eulerian grids. Aly [27] modeled the multi-phase flow and natural convection in a square/cubic cavity using ISPH method in two and three dimensions. Rayleigh-Taylor instability between two and three adjacent fluid layers has been simulated and also the natural convection in a square/cubic cavity has been introduced with a good agreement compared to benchmark tests. Aly and Asai [28] modeled non-Darcy flows through porous media using an extended ISPH method. In their study, unsteady lid-Driven flow, natural convection in non-Darcy porous cavities and natural convection in porous medium-fluid interface are examined separately by using ISPH method. In addition, Aly and Ahmed [29] modeled the non-Darcy flows through anisotropic porous media for natural/mixed convection and heat transfer in a cavity using ISPH method. They studied unsteady natural/mixed convection in non-Darcy porous cavities using both ISPH method and Finite Volume Method. The objective of this study was to present ISPH method to model the double-diffusive natural convection in an enclosure filled with nanofluid. In this study, the model used for the binary nanofluid incorporates the effects of Brownian motion and thermophoresis. In addition, the thermal energy equations include regular diffusion and cross-diffusion terms. The results are presented with flow configurations, isotherms, concentration and nanoparticle volume fraction contours and average Nusselt and Sherwood numbers for different cases. The results from this investigation are well validated and have favorable comparisons with previously published results. It is found that, among all cases, a good natural convection can be obtained by considering the double diffusive case.

2. Problem description

Fig. 1 shows the physical model for the current problem for the natural convection in an enclosure filled with nanofluid. It is assumed that, the vertical walls are kept at constant temperatures, T_h and T_l, constant masses C_h and C_l and constant nanoparticle volume fraction ϕ_h and ϕ_l where, $T_h > T_l$, $C_h > C_l$ and $\phi_h > \phi_l$. However, the horizontal walls are adiabatic. Thermophoresis and Brownian motion effects are included in these assumptions.

3. Mathematical analysis

Here, we used mathematical nanofluid model proposed by Buongiorno [30] for nanofluid in combination with thermo-diffusion and the Boussinesq approximation for the buoyancy force. The water is assumed as a base fluid and the solid nanoparticles are in thermal equilibrium. Boussinesq approximation is used to determine the variation of density in the buoyancy term where the other thermo-physical properties of the nanofluid are assumed constant. The continuity, momentum, energy and concentration equations for the unsteady natural convection in the two-dimensional enclosure can be written in dimensional form [27–29] as follows:

$$\frac{\partial u}{\partial x}+\frac{\partial \mathrm{v}}{\partial y}=0, \tag{1}$$

$$\frac{\partial u}{\partial t}+u\frac{\partial u}{\partial x}+\mathrm{v}\frac{\partial u}{\partial y}=\frac{1}{\rho_f}\left(-\frac{\partial p}{\partial x}+\mu_f\left(\frac{\partial^2 u}{\partial x^2}+\frac{\partial^2 u}{\partial y^2}\right)\right), \tag{2}$$

$$\frac{\partial \mathrm{v}}{\partial t}+u\frac{\partial \mathrm{v}}{\partial x}+\mathrm{v}\frac{\partial \mathrm{v}}{\partial y} = \frac{1}{\rho_f}\begin{pmatrix} -\frac{\partial p}{\partial y}+\mu_f\left(\frac{\partial^2 \mathrm{v}}{\partial x^2}+\frac{\partial^2 \mathrm{v}}{\partial y^2}\right)+(1-\phi_l)\rho_f g\beta_T(T-T_l)+ \\ (1-\phi_l)\rho_f g\beta_C(C-C_l)-(\rho_p-\rho_f)g(\phi-\phi_l) \end{pmatrix}, \tag{3}$$

$$(\rho c)_f\left(\frac{\partial T}{\partial t}+u\frac{\partial T}{\partial x}+\mathrm{v}\frac{\partial T}{\partial y}\right)=k_f\left(\frac{\partial^2 T}{\partial x^2}+\frac{\partial^2 T}{\partial y^2}\right) + (\rho c)_p\left[D_B\left(\frac{\partial \phi}{\partial x}\frac{\partial T}{\partial x}+\frac{\partial \phi}{\partial y}\frac{\partial T}{\partial y}\right)+\frac{D_T}{T_m}\left(\left(\frac{\partial T}{\partial x}\right)^2+\left(\frac{\partial T}{\partial y}\right)^2\right)\right] + (\rho c)_f D_{TC}\left(\frac{\partial^2 C}{\partial x^2}+\frac{\partial^2 C}{\partial y^2}\right), \tag{4}$$

$$\frac{\partial C}{\partial t}+u\frac{\partial C}{\partial x}+\mathrm{v}\frac{\partial C}{\partial y}=D_S\left(\frac{\partial^2 C}{\partial x^2}+\frac{\partial^2 C}{\partial y^2}\right)+D_{CT}\left(\frac{\partial^2 T}{\partial x^2}+\frac{\partial^2 T}{\partial y^2}\right), \tag{5}$$

$$\frac{\partial \phi}{\partial t}+u\frac{\partial \phi}{\partial x}+\mathrm{v}\frac{\partial \phi}{\partial y}=D_B\left(\frac{\partial^2 \phi}{\partial x^2}+\frac{\partial^2 \phi}{\partial y^2}\right)+\frac{D_T}{T_m}\left(\frac{\partial^2 T}{\partial x^2}+\frac{\partial^2 T}{\partial y^2}\right). \tag{6}$$

where u and v are the velocity components in the x- and y-directions. p is the fluid pressure, T is the temperature, C is the solute concentration. ρ_f is the density of the base fluid and μ, k, β_T and β_C are the viscosity, thermal conductivity, volumetric thermal expansion coefficient and volumetric solutal expansion coefficient of the nanofluid.

The following dimensionless parameters are used to convert Eqs. (1)–(6) to non-dimensional forms:

$$X=\frac{x}{W},\quad Y=\frac{y}{W},\quad \tau=\frac{t\alpha_f}{W^2},\quad U=\frac{uW}{\alpha_f},\quad V=\frac{\mathrm{v}W}{\alpha_f},$$
$$P=\frac{pW^2}{\rho_f\alpha_f^2},\quad \theta=\frac{T-T_l}{\Delta T}-0.5(H-W),\quad Ra=\frac{\mathrm{g}\beta_f W^3\Delta T}{v\alpha_f},$$
$$Pr=\frac{v}{\alpha_f},\quad \Phi=\frac{C-C_l}{\Delta C}-0.5(H-W),$$
$$\varphi=\frac{\phi-\phi_l}{\Delta\phi}-0.5(H-W), \tag{7}$$

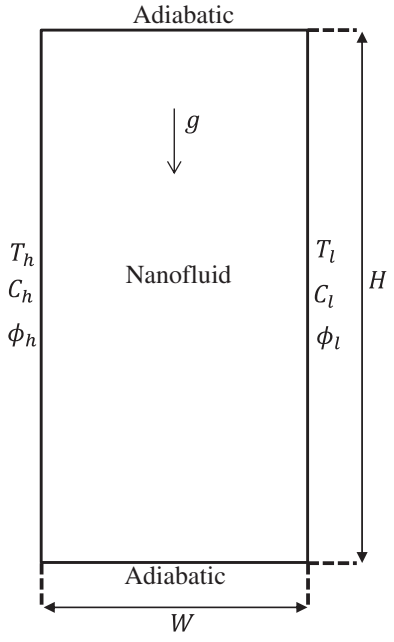

Figure 1 Boundary condition for natural convection in an enclosure filled with nanofluid.

Then, the dimensionless continuity, momentum, energy and mass equations are written as follows:

$$\frac{\partial U}{\partial X}+\frac{\partial V}{\partial Y}=0, \tag{8}$$

$$\frac{\partial U}{\partial \tau}+U\frac{\partial U}{\partial X}+V\frac{\partial U}{\partial Y}=-\frac{\partial P}{\partial X}+Pr\left(\frac{\partial^2 U}{\partial X^2}+\frac{\partial^2 U}{\partial Y^2}\right), \tag{9}$$

$$\frac{\partial V}{\partial \tau}+U\frac{\partial V}{\partial X}+V\frac{\partial V}{\partial Y}=-\frac{\partial P}{\partial Y}+Pr\left(\frac{\partial^2 V}{\partial X^2}+\frac{\partial^2 V}{\partial Y^2}\right)+Ra_T\cdot Pr[\theta+Ra_{Tc}\Phi-Nr\varphi], \tag{10}$$

$$\frac{\partial \theta}{\partial \tau}+U\frac{\partial \theta}{\partial X}+V\frac{\partial \theta}{\partial Y}=\left(\frac{\partial^2 \theta}{\partial X^2}+\frac{\partial^2 \theta}{\partial Y^2}\right)+Nb\left(\frac{\partial \varphi}{\partial X}\frac{\partial \theta}{\partial X}+\frac{\partial \varphi}{\partial Y}\frac{\partial \theta}{\partial Y}\right)+Nt\left(\left(\frac{\partial \theta}{\partial X}\right)^2+\left(\frac{\partial \theta}{\partial Y}\right)^2\right)+Nd\left(\frac{\partial^2 \Phi}{\partial X^2}+\frac{\partial^2 \Phi}{\partial Y^2}\right), \tag{11}$$

$$\frac{\partial \Phi}{\partial \tau}+U\frac{\partial \Phi}{\partial X}+V\frac{\partial \Phi}{\partial Y}=\frac{1}{Le}\left(\frac{\partial^2 \Phi}{\partial X^2}+\frac{\partial^2 \Phi}{\partial Y^2}\right)+Sr\left(\frac{\partial^2 \theta}{\partial X^2}+\frac{\partial^2 \theta}{\partial Y^2}\right), \tag{12}$$

$$\frac{\partial \varphi}{\partial \tau}+U\frac{\partial \varphi}{\partial X}+V\frac{\partial \varphi}{\partial Y}=\frac{1}{Ln}\left(\frac{\partial^2 \varphi}{\partial X^2}+\frac{\partial^2 \varphi}{\partial Y^2}\right)+\frac{Nt}{LnNb}\left(\frac{\partial^2 \theta}{\partial X^2}+\frac{\partial^2 \theta}{\partial Y^2}\right), \tag{13}$$

where the various parameters are defined as follows: $Ra_T=\frac{(1-\phi_l)g\beta_T W^3\Delta T}{\nu\alpha_f}$ is thermal Rayleigh number. $Ra_{Tc}=Ra_c/Ra_T$ is concentration Rayleigh number to thermal Rayleigh number ratio. $Nr=\frac{(\rho_p-\rho_f)\Delta\phi}{(1-\phi_l)\beta_T\alpha_f\Delta T}$ is buoyancy ratio for nanofluid. $Nt=\frac{D_T\Delta T(\rho c)_p}{T_m\alpha_f(\rho c)_f}$ is thermophoresis parameter. $Nb=\frac{(\rho c)_p D_B\Delta\phi}{\alpha_f(\rho c)_f}$ is Brownian motion parameter. $Nd=\frac{D_{TC}\Delta C}{\alpha_f\Delta T}$ is modified Dufour parameter. $Le=\frac{\alpha_f}{D_S}$ is regular Lewis number. $Sr=\frac{D_{CT}\Delta T}{\alpha_f\Delta C}$ is Soret parameter. $Ln=\frac{\alpha_f}{D_B}$ is nanofluid Lewis number.

In this, the boundary conditions have been introduced in dimensionless form as follows:

$$\begin{aligned}
&U=0;\ V=0;\ \theta=0.5,\ \Phi=0.5,\ \varphi=0.5\ \text{ for } X=0,\ 0\leqslant Y\leqslant 2,\\
&U=0;\ V=0;\ \theta=-0.5,\ \Phi=-0.5,\ \varphi=-0.5\ \text{ for } X=1,\ 0\leqslant Y\leqslant 2,\\
&U=0;\ V=0;\ \frac{\partial\theta}{\partial X}=0,\ \frac{\partial\Phi}{\partial X}=0,\ \frac{\partial\varphi}{\partial X}=0\ \text{ for } Y=0,\ 0\leqslant X\leqslant 1,\\
&U=0;\ V=0;\ \frac{\partial\theta}{\partial X}=0,\ \frac{\partial\Phi}{\partial X}=0,\ \frac{\partial\varphi}{\partial X}=0\ \text{ for } Y=2,\ 0\leqslant X\leqslant 1.
\end{aligned} \tag{14}$$

The local Nusselt number and local Sherwood number can be defined as follows:

$$Nu=-\left.\frac{\partial\theta}{\partial X}\right|_{X=0}, \tag{15}$$

$$Sh=-\left.\frac{\partial\Phi}{\partial X}\right|_{X=0}. \tag{16}$$

For the majority of design problems, the knowledge of the average Nusselt number is very useful. The average Nusselt number and average Sherwood number are obtained through the following integration:

$$\overline{Nu}=-\frac{1}{A}\int_0^A\left(\frac{\partial\theta}{\partial X}\right)dY. \tag{17}$$

$$\overline{Sh}=-\frac{1}{A}\int_0^A\left(\frac{\partial\Phi}{\partial X}\right)dY \tag{18}$$

where $A=H/W$ is the enclosure aspect ratio.

4. ISPH method

The ISPH algorithm is implemented in a semi-implicit form in order to solve the incompressible viscous flow equations. In this section, the procedure for the solution of governing non-dimensional equations is described.

The ISPH method is based on the calculation of an intermediate velocity from a momentum equation where the pressure gradients are omitted. Then, the pressure is evaluated through solving the pressure Poisson equation (PPE). The PPE after SPH interpolation is solved by a preconditioned diagonal scaling Conjugate Gradient PCG method [31] with a convergence tolerance ($=1.0\times10^{-9}$). Finally, the velocity is corrected using the evaluated pressure.

4.1. Temporal discretization

The momentum equation can be discretized in time using predictor-corrector scheme. Here, the momentum, energy and concentration equations are described in Lagrangian description. In particular, the time discrete momentum equation in its semi-implicit form can be written as follows:

$$\left[\frac{U^{n+1}-U^n}{\Delta t}\right]=-\left(\frac{\partial P}{\partial X}\right)^{n+1}+Pr\left(\frac{\partial^2 U}{\partial X^2}+\frac{\partial^2 U}{\partial Y^2}\right)^n, \tag{19}$$

$$\left[\frac{V^{n+1}-V^n}{\Delta t}\right] = -\left(\frac{\partial P}{\partial Y}\right)^{n+1} + Pr\left(\frac{\partial^2 V}{\partial X^2}+\frac{\partial^2 V}{\partial Y^2}\right)^n + Ra_T Pr(\theta^n + Ra_{Tc}\Phi^n - Nr\varphi^n), \quad (20)$$

Step 1: Predict the velocity

The first step of the predictor-corrector scheme is the calculation of an intermediate velocity (U^*, V^*) from the momentum equation without including the pressure terms. Thus, the following equations are obtained:

$$U^* = U^n + \Delta t\left(Pr\left(\frac{\partial^2 U}{\partial X^2}+\frac{\partial^2 U}{\partial Y^2}\right)^n\right), \quad (21)$$

$$V^* = V^n + \Delta t\left(Pr\left(\frac{\partial^2 V}{\partial X^2}+\frac{\partial^2 V}{\partial Y^2}\right)^n + Ra_T Pr(\theta^n + Ra_{Tc}\Phi^n - Nr\varphi^n)\right). \quad (22)$$

Step 2: Solving the pressure Poisson equation

In the second step, the pressure is calculated using the modified Poisson equation, which ensures that the continuity equation is satisfied and for the generalized model can be written as follows:

$$\frac{\partial^2 P^{n+1}}{\partial X^2}+\frac{\partial^2 P^{n+1}}{\partial Y^2} = \left(\frac{1}{\Delta t}\left(\frac{\partial U^*}{\partial X}\right)+\frac{1}{\Delta t}\left(\frac{\partial V^*}{\partial Y}\right)\right) + \gamma\frac{\rho^0 - \langle\rho^*\rangle}{\rho^0\Delta t^2}, \quad (23)$$

Note, the relaxation coefficient γ, $(0 \leqslant \gamma \leqslant 1)$ can be decided from pre-analysis calculation. In this study, the particle size d_0 is taken as 2.0 cm and then the relaxation coefficient is decided as $\gamma = 0.25$ according to Asai et al. [19].

Step 3: Corrected velocity

In the third step, the real velocity values are obtained using the following correction:

$$U^{n+1} = U^* - \Delta t\left[\frac{\partial P}{\partial X}\right]^{n+1}, \quad (24)$$

$$V^{n+1} = V^* - \Delta t\left[\frac{\partial P}{\partial Y}\right]^{n+1}, \quad (25)$$

Step 4: Thermal flow problems:

In this step, the time discretization of the energy equation is introduced:

$$\left(\frac{\theta^{n+1}-\theta^n}{\Delta\tau}\right) = \left(\frac{\partial^2\theta}{\partial X^2}+\frac{\partial^2\theta}{\partial Y^2}\right)^n + Nb\left(\frac{\partial\varphi}{\partial X}\frac{\partial\theta}{\partial X}+\frac{\partial\varphi}{\partial Y}\frac{\partial\theta}{\partial Y}\right)^n + Nt\left(\left(\frac{\partial\theta}{\partial X}\right)^2+\left(\frac{\partial\theta}{\partial Y}\right)^2\right)^n + Nd\left(\frac{\partial^2\Phi}{\partial X^2}+\frac{\partial^2\Phi}{\partial Y^2}\right)^n, \quad (26)$$

Step 5: Concentration flow problems:

In this step, the time discretization of the concentration equation is introduced:

$$\left(\frac{\Phi^{n+1}-\Phi^n}{\Delta\tau}\right) = \frac{1}{Le}\left(\frac{\partial^2\Phi}{\partial X^2}+\frac{\partial^2\Phi}{\partial Y^2}\right)^n + Sr\left(\frac{\partial^2\theta}{\partial X^2}+\frac{\partial^2\theta}{\partial Y^2}\right)^n, \quad (27)$$

Step 6: Nanoparticle volume fraction problems:

$$\left(\frac{\varphi^{n+1}-\varphi^n}{\Delta\tau}\right) = \frac{1}{Ln}\left(\frac{\partial^2\varphi}{\partial X^2}+\frac{\partial^2\varphi}{\partial Y^2}\right)^n + \frac{Nt}{LnNb}\left(\frac{\partial^2\theta}{\partial X^2}+\frac{\partial^2\theta}{\partial Y^2}\right)^n. \quad (28)$$

4.2. SPH formulations

A spatial discretization using scattered particles, which is based on the SPH, is summarized. First, a physical scalar function $A(X_i)$ at a sampling point X_i can be represented by the following integral form:

$$A(X_i) = \int W(X_i - X_j, h)A(X_i)d\Omega = \int W(R_{ij}, h)A(X_j)d\Omega, \quad (29)$$

where W is a weight function called by smoothing kernel function in the SPH literature. In the smoothing kernel function, $R_{ij} = |X_i - X_j|$ and h are the distance between neighbor particles and smoothing length (which is taken as 1.2 times the initial particle size), respectively. For SPH numerical analysis, the integral Eq. (29) is approximated by a summation of contributions from neighbor particles in the support domain.

Table 1 The analysis parameters for double-diffusive natural convection in an enclosure.

Number of particles	5775
Initial particle distance	0.02 m
Time step	0.0001 sec
Relaxation coefficient (γ)	0.25
Boundary condition	Non-slip

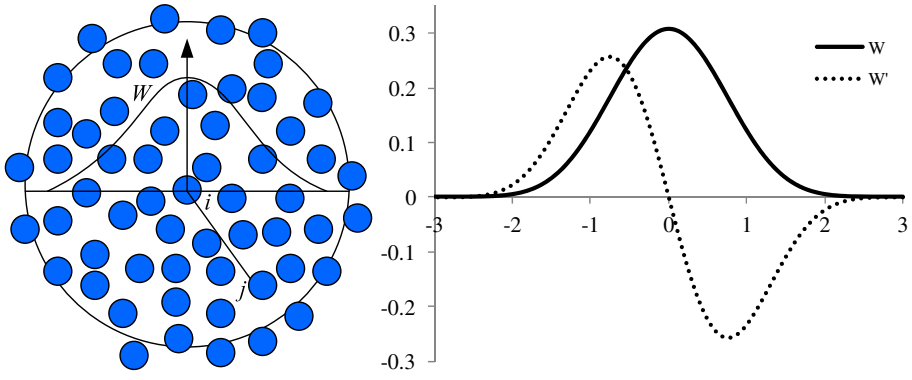

Figure 2 Particle approximations in support domain (left) and the quintic kernel function with its first derivative (right).

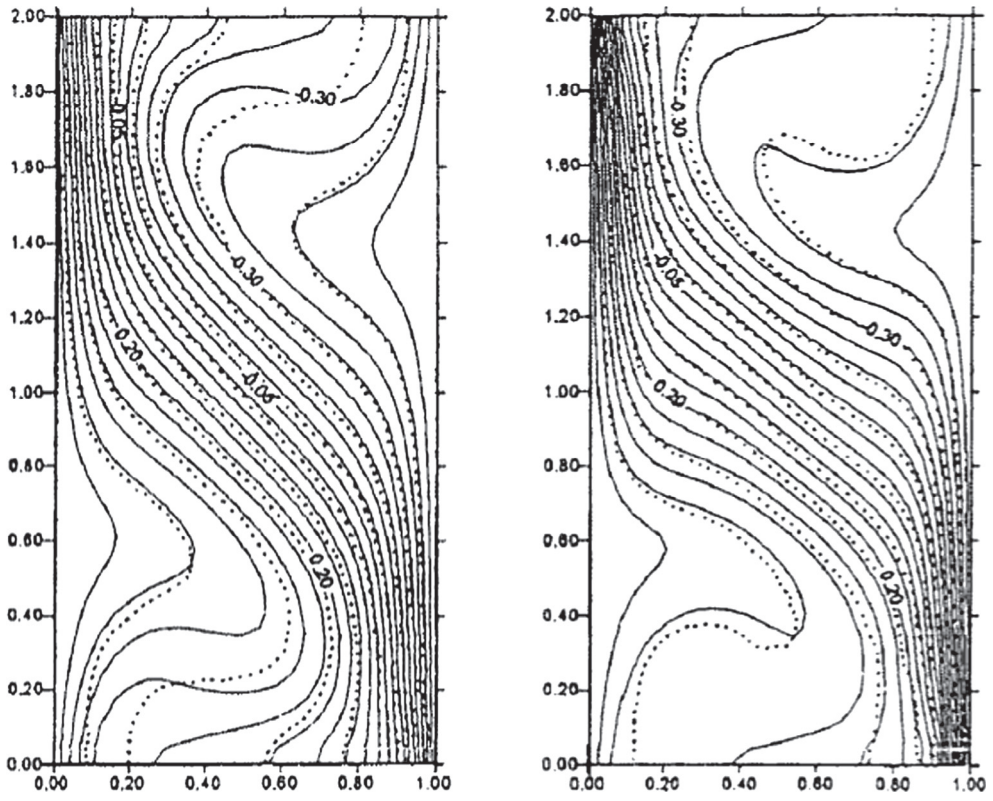

(----) Nishimura et al. [32] and (—) Chamkha [33].

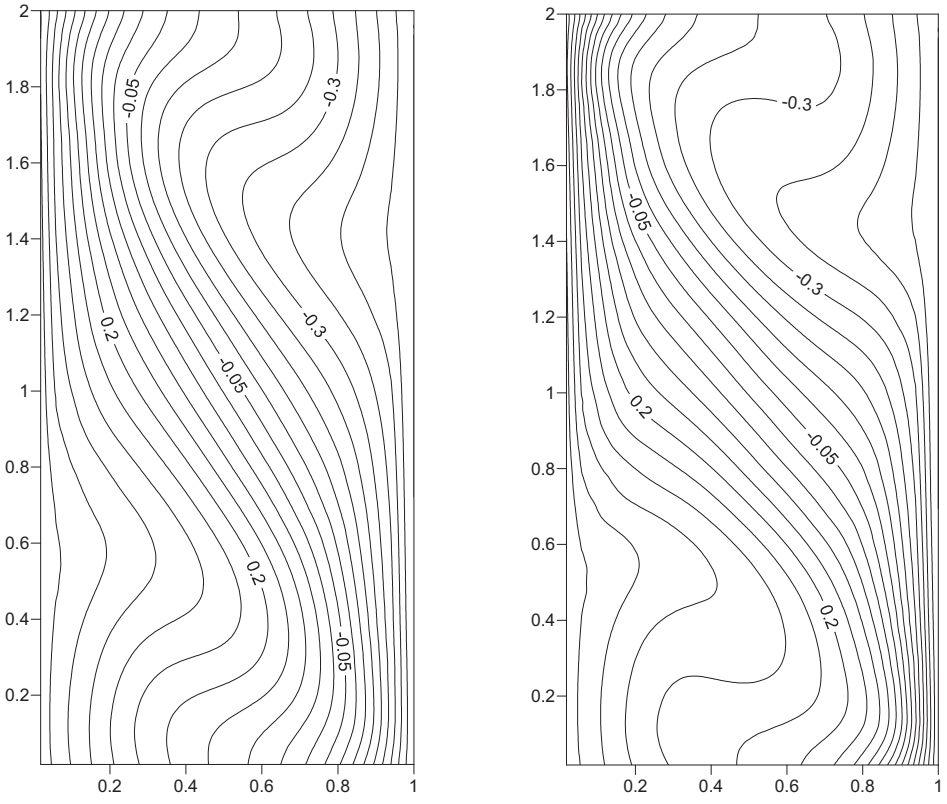

ISPH method

(a) Isotherms (b) Concentration contours

Figure 3 Comparison of compositional-dominated solution with Nishimura et al. [32] and Chamkha [33] for $Le = 2.0$, $N = 1.3$, $Pr = 1.0$ and $Ra = 10^5$.

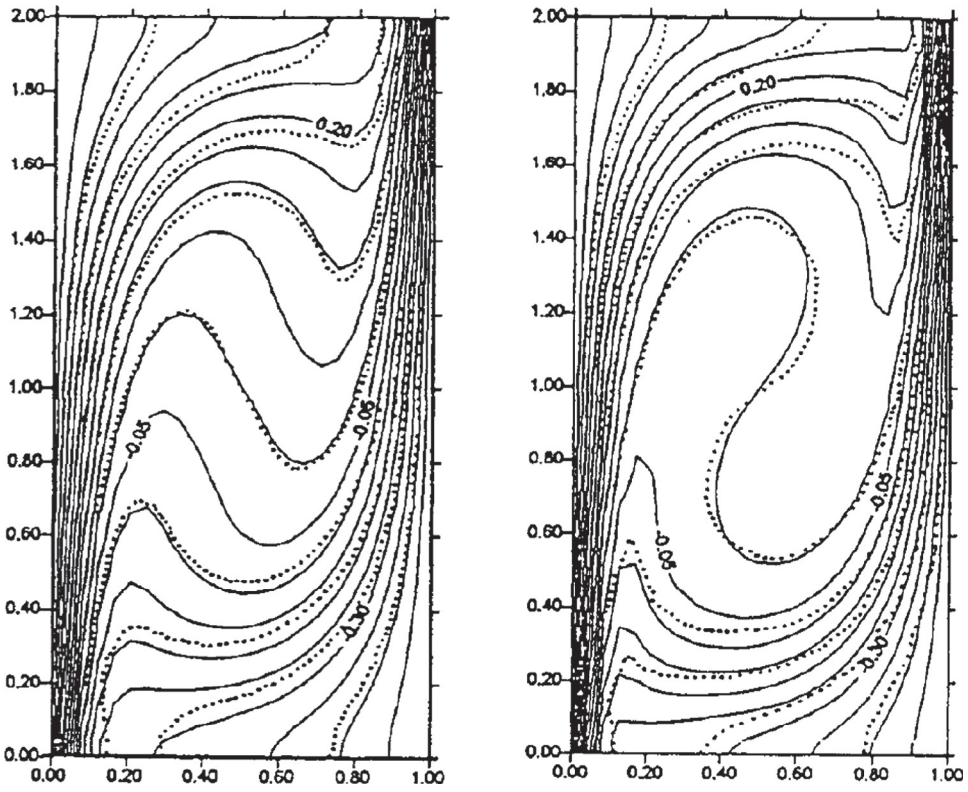

(----) Nishimura et al. [32] and (—) Chamkha [33].

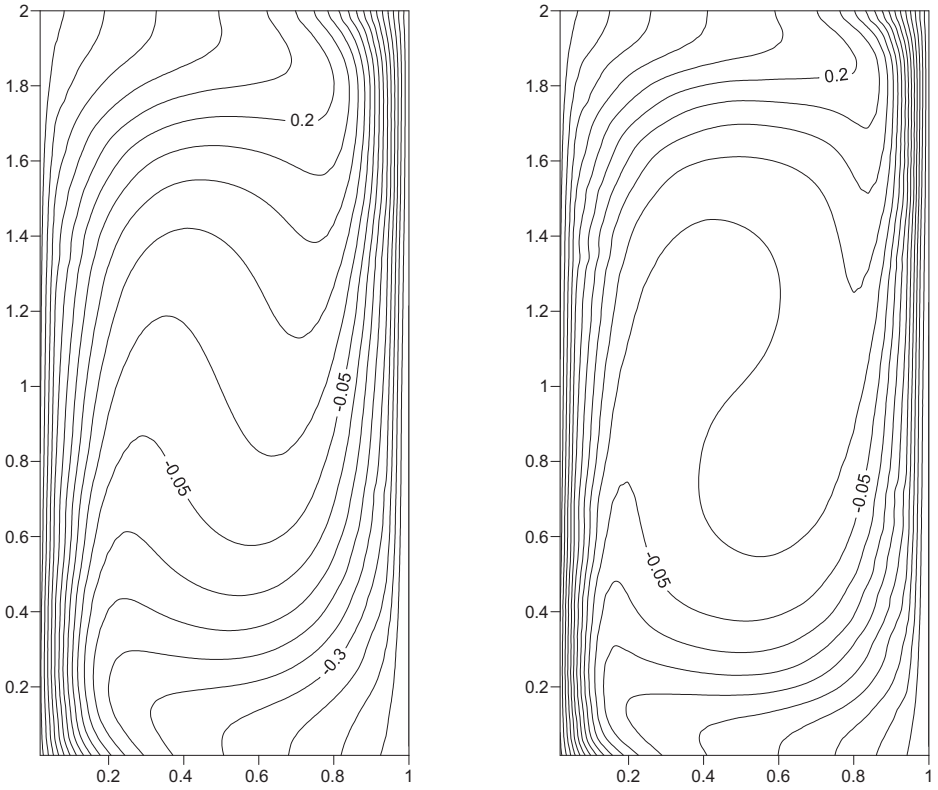

ISPH method

(a) Isotherms (b) Concentration contours

Figure 4 Comparison of thermal-dominated solution with Nishimura et al. [32] and Chamkha [33] for $Le = 2.0$, $N = 0.8$, $Pr = 1.0$ and $Ra = 10^5$.

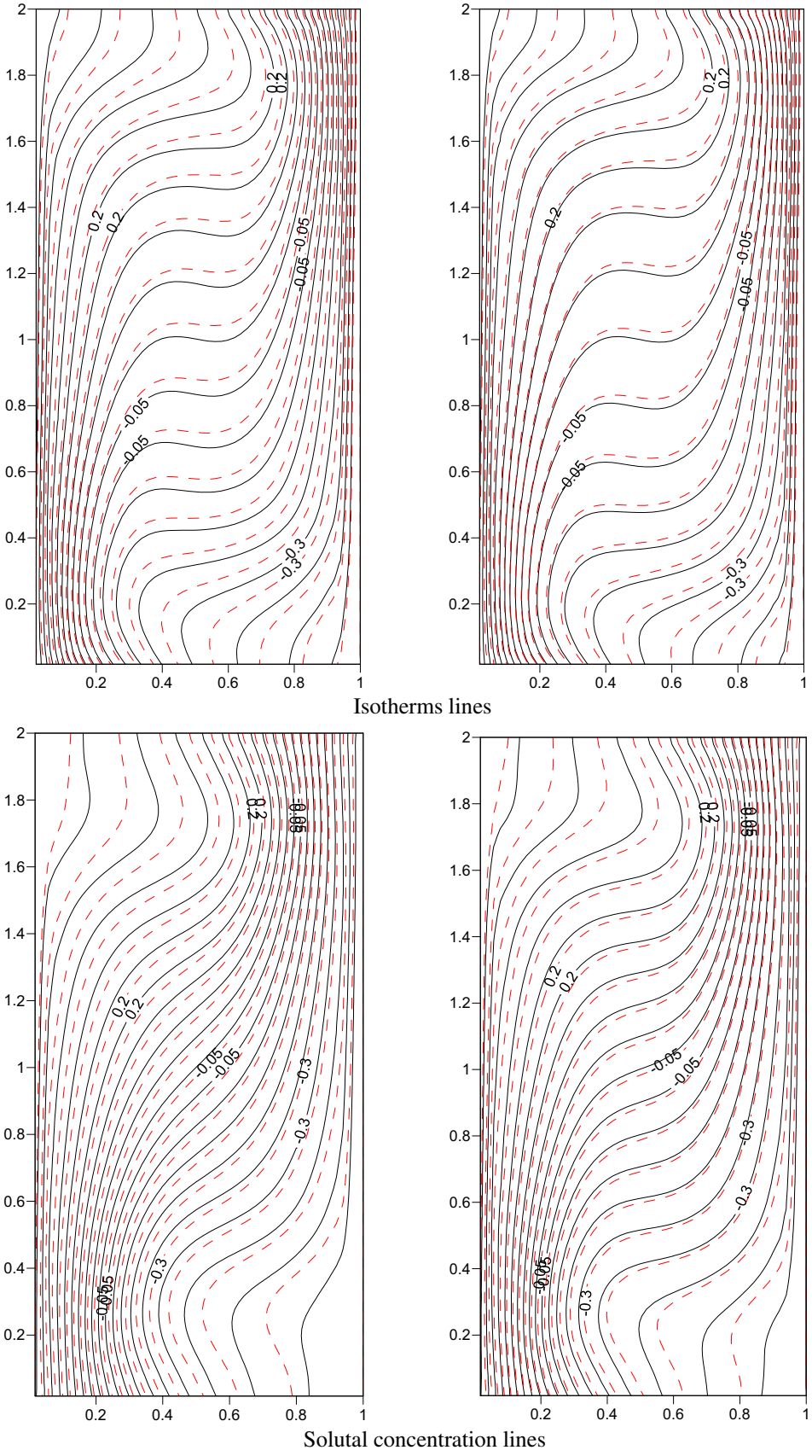

Figure 5 Isotherms, concentration and rescaled nanoparticle volume fraction lines and contours of horizontal and vertical velocities, respectively for (—) regular fluid and (----) nanofluid at $Ra = 10^4$, $Le = 1.0$, $Ln = 10$ and $Sr = 1.0$.

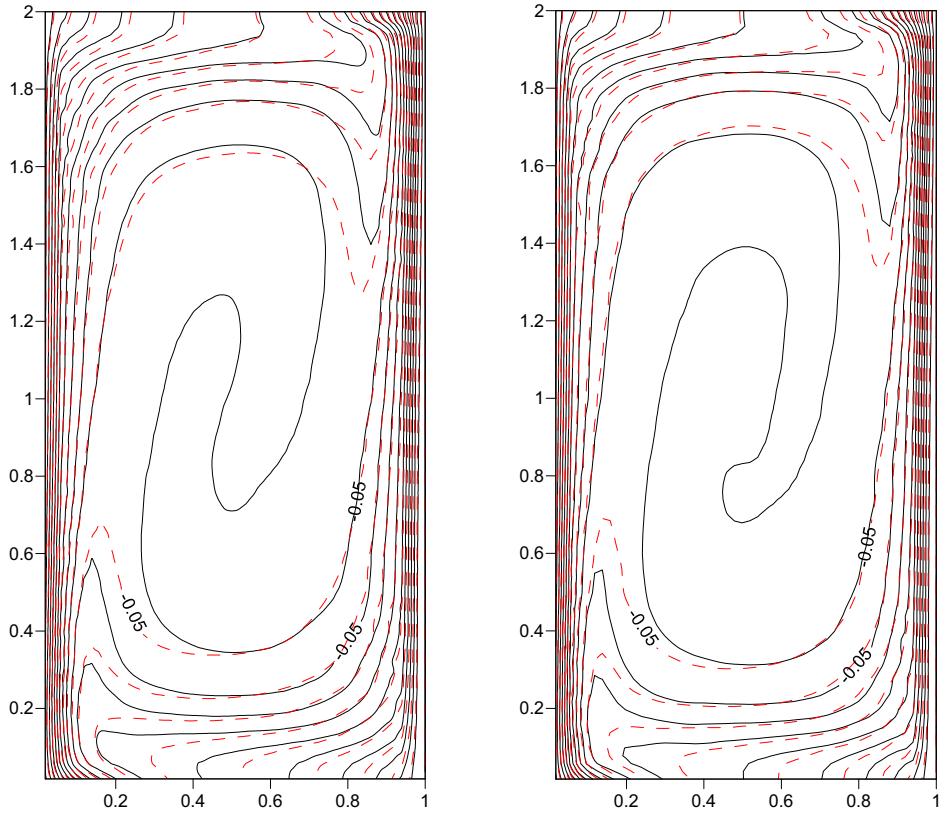

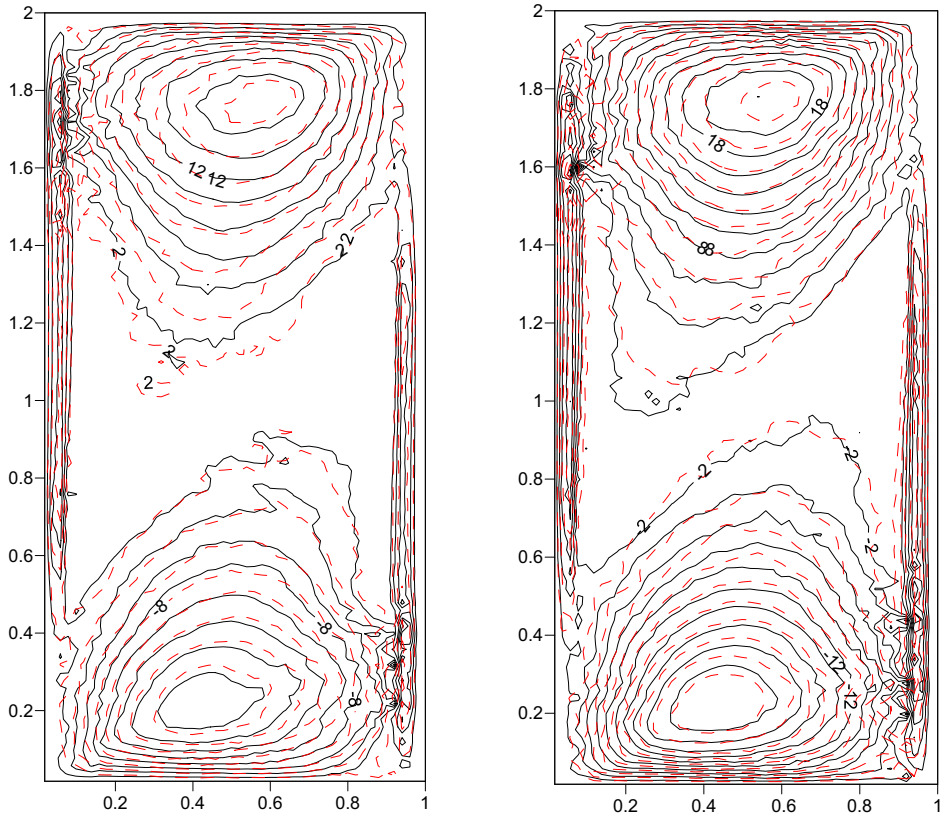

Fig. 5 (*continued*)

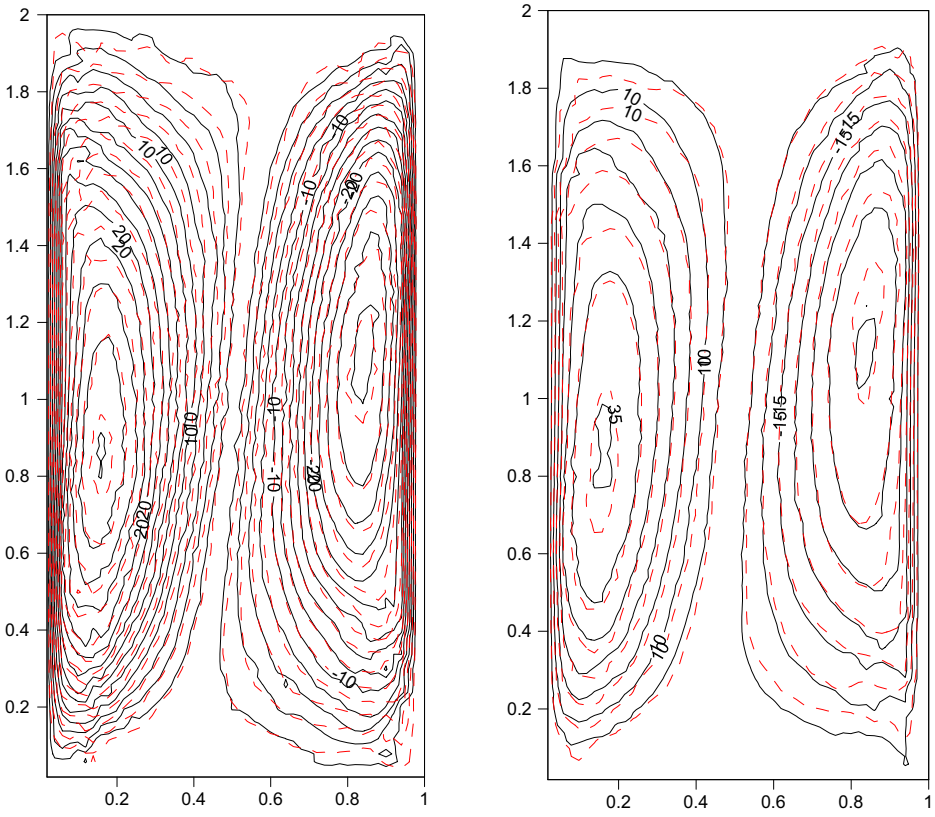

Fig. 5 (*continued*)

$$A(X_i) \approx \langle A_i \rangle = \sum_j \frac{m_j}{\rho_j} W(R_{ij}, h) A(X_j), \tag{30}$$

where the subscripts i and j indicate positions of labeled particle, ρ_j and m_j mean density and representative mass related to particle j, respectively. Note that, the triangle bracket $\langle A_i \rangle$ means SPH approximation of a function A. The gradient of the scalar function can be assumed by using the above defined SPH approximation as follows:

$$\nabla A(X_i) \approx \langle \nabla A_i \rangle = \frac{1}{\rho_i} \sum_j m_j (A_j - A_i) \nabla W(R_{ij}, h), \tag{31}$$

Also, the other expression for the gradient can be represented by

$$\nabla A(X_i) \approx \langle \nabla A_i \rangle = \rho_i \sum_j m_j \left(\frac{A_j}{\rho_j^2} + \frac{A_i}{\rho_i^2} \right) \nabla W(R_{ij}, h), \tag{32}$$

In this paper, we used quintic spline function as a kernel function:

$$W(q,h) = \beta_d \begin{cases} (3-q)^5 - 6(2-q)^5 + 15(1-q)^5, & 0 \leqslant q < 1, \\ (3-q)^5 - 6(2-q)^5, & 1 \leqslant q < 2, \\ (3-q)^5, & 2 \leqslant q < 3, \\ 0, & q \geqslant 3, \end{cases} \tag{33}$$

where $q = R_{ij}/h$, β_d is $7/478\pi h^2$ and $3/358\pi h^3$, respectively, in two- and three dimensional space. The particle approximations in support domain and the quintic kernel function with its first derivative are shown in Fig. 2.

4.3. Projection-based ISPH formulations

Here, the projection method for incompressible fluid problem, which is summarized in Section 4, is discretized into particle quantities based on the SPH methodology. For this purpose, the gradient of pressure and the divergence of velocity are approximated as follows:

$$\langle \nabla P(\boldsymbol{x}_i) \rangle = \rho_i \sum_j m_j \left(\frac{P_i}{\rho_i^2} + \frac{P_j}{\rho_j^2} \right) \nabla W_{ij}, \tag{34}$$

$$\langle \nabla \cdot \boldsymbol{U}(\boldsymbol{x}_i) \rangle = \sum_j \frac{m_j}{\rho_j} (\boldsymbol{U}(\boldsymbol{x}_j) - \boldsymbol{U}(\boldsymbol{x}_i)) \nabla W_{ij}, \tag{35}$$

The second derivative of velocity and the Laplacian of pressure have been proposed by Morris et al. [17] by an approximation expression as follows:

$$\langle \nabla^2 \boldsymbol{U}(\boldsymbol{x}_i) \rangle = \sum_j m_j \left(\frac{\rho_i + \rho_j}{\rho_i \rho_j} \frac{R_{ij} \cdot \nabla W_{ij}}{R_{ij}^2 + \eta^2} \right) (\boldsymbol{V}(\boldsymbol{x}_j) - \boldsymbol{V}(\boldsymbol{x}_i)), \tag{36}$$

where η is a parameter to avoid a zero dominator, and its value is usually given by $\eta^2 = 0.0001 h^2$.

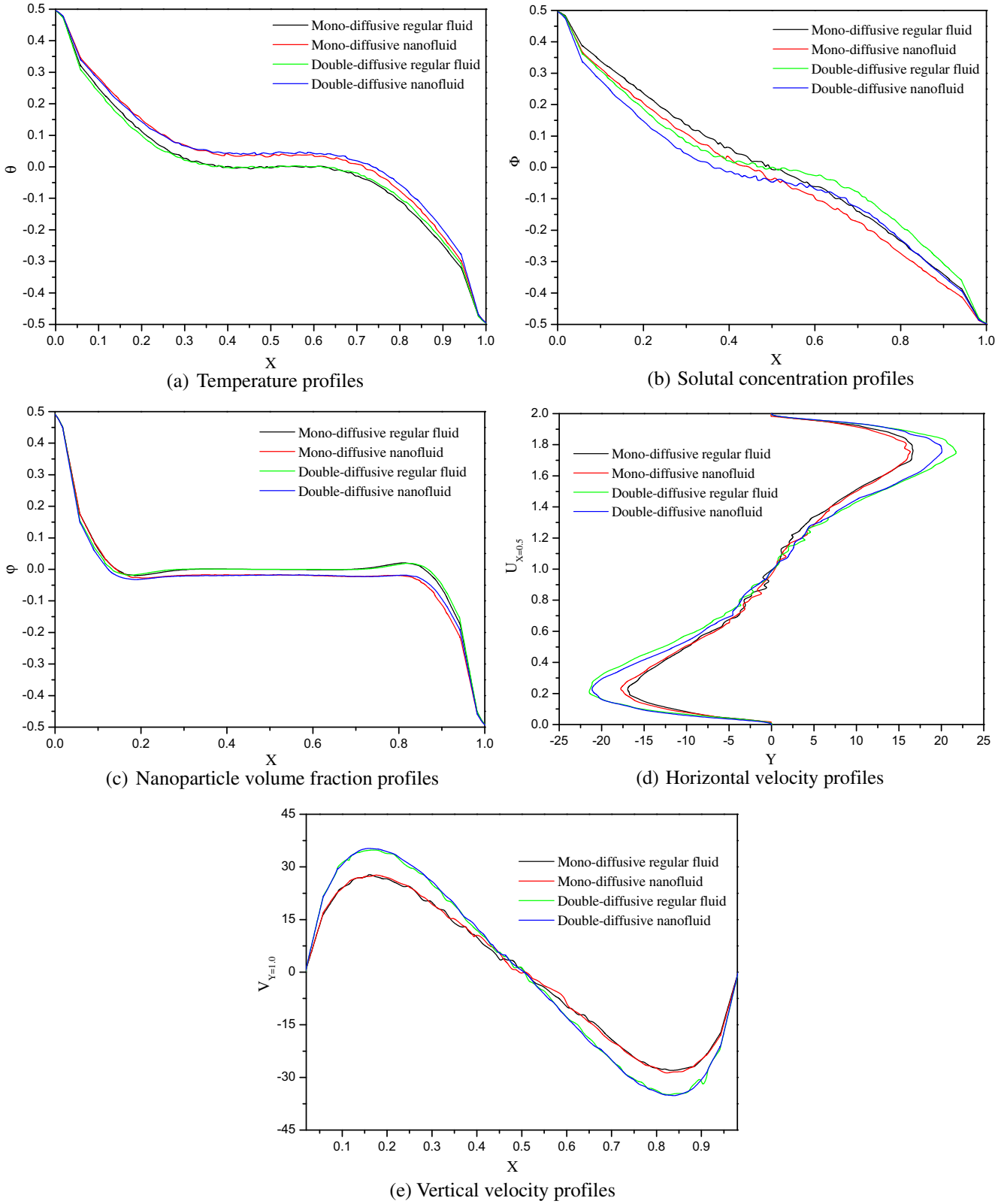

(a) Temperature profiles

(b) Solutal concentration profiles

(c) Nanoparticle volume fraction profiles

(d) Horizontal velocity profiles

(e) Vertical velocity profiles

Figure 6 The temperature, solutal concentration, nanoparticle volume fraction, horizontal and vertical velocities, respectively for four cases, mono-diffusive regular fluid, mono-diffusive nanofluid, double-diffusive regular fluid and double-diffusive nanofluid at $Ra = 10^4$, $Le = 1.0$, $Ln = 10$ and $Sr = 1.0$.

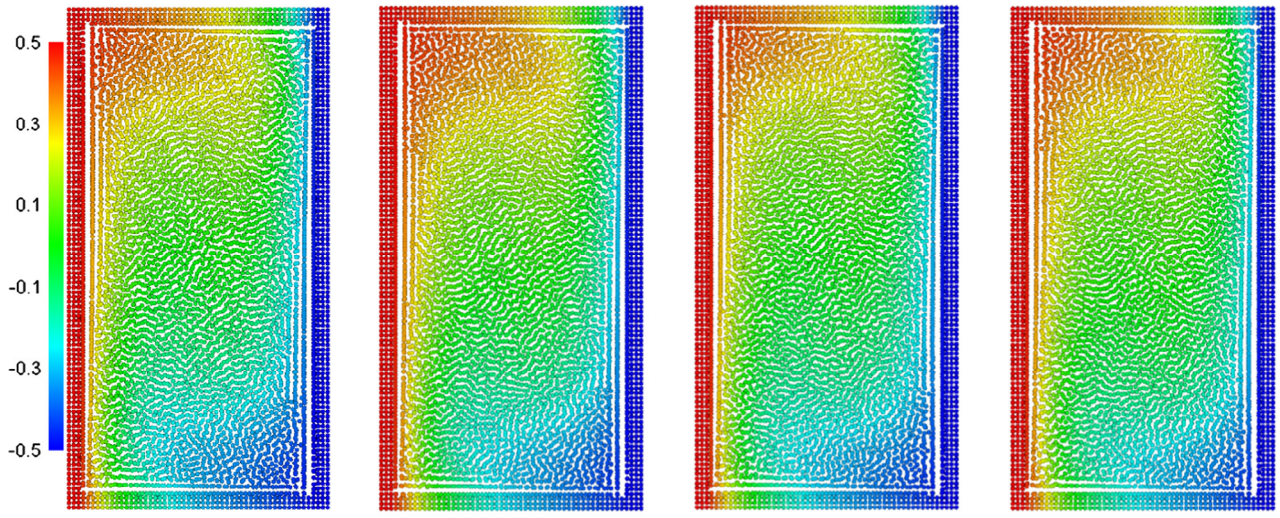

(a) Temperature distribution

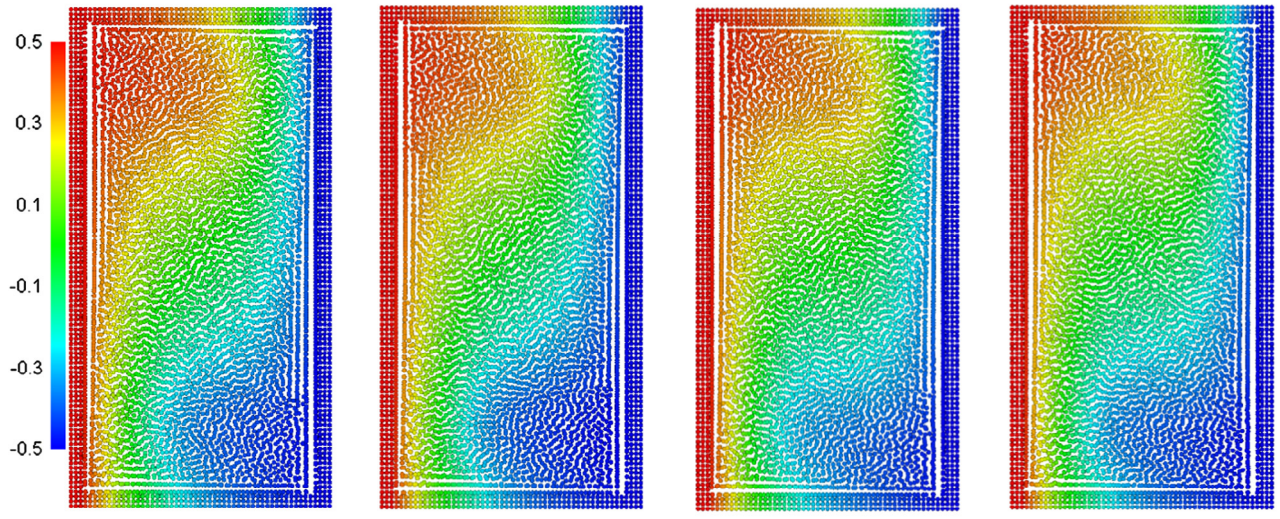

(b) Solutal concentration distribution

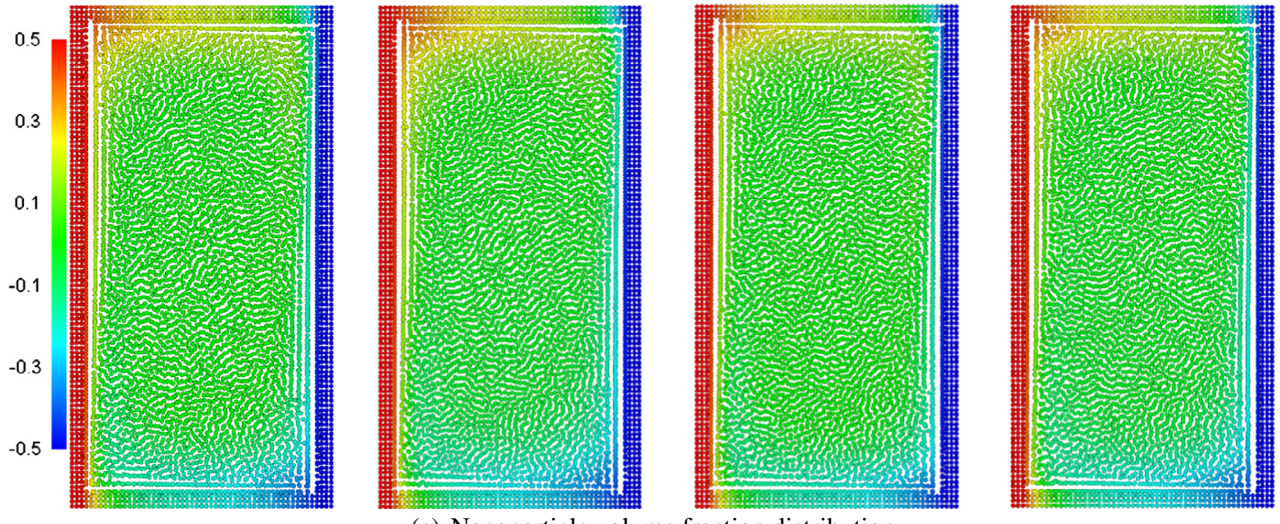

(c) Nanoparticle volume fraction distribution

Figure 7 The snapshots of the temperature, solutal concentration, nanoparticle volume fraction, horizontal and vertical velocities, respectively at steady state for four cases, mono-diffusive regular fluid, mono-diffusive nanofluid, double-diffusive regular fluid and double-diffusive nanofluid at $Ra = 10^4$, $Le = 1.0$, $Ln = 10$ and $Sr = 1.0$.

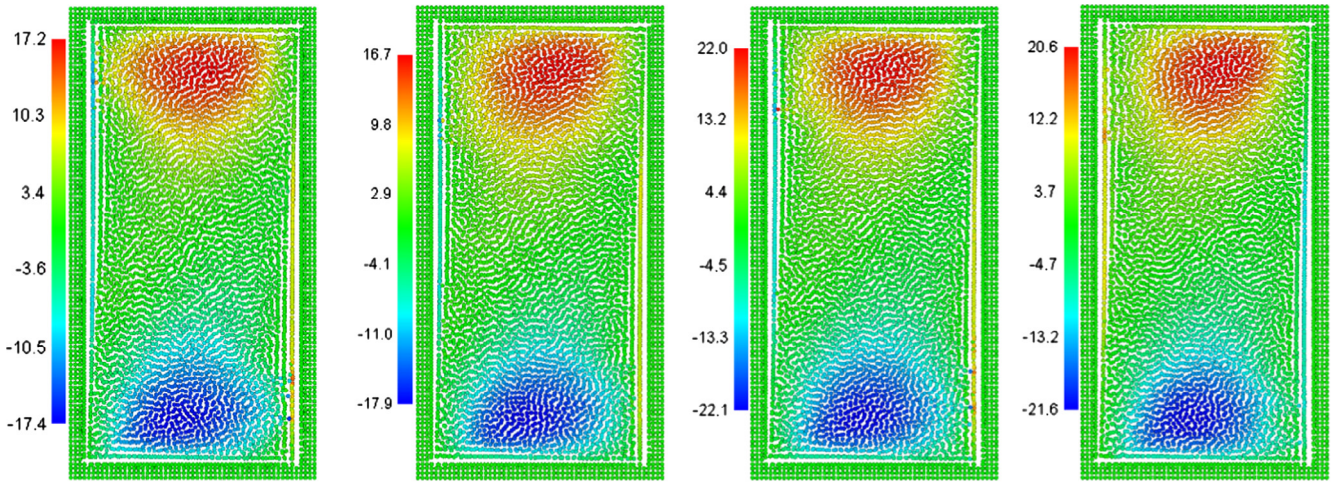

(d) Horizontal velocity distribution

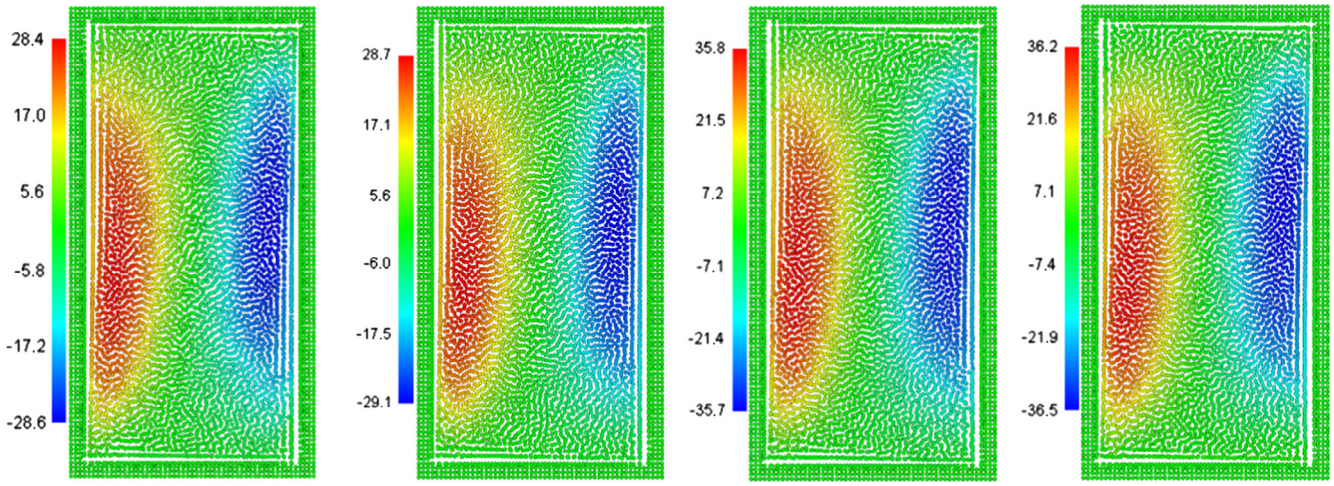

(e) Vertical velocity distribution

Mono-diffusive regular fluid | Mono-diffusive nanofluid | Double-diffusive regular fluid | Double-diffusive nanofluid

Fig. 7 (*continued*)

$$\langle \nabla^2 P(\boldsymbol{x}_i) \rangle = \sum_j m_j \left(\frac{\rho_i + \rho_j}{\rho_i \rho_j} \frac{P_{ij} R_{ij} \cdot \nabla W_{ij}}{R_{ij}^2 + \eta^2} \right), \tag{37}$$

The PPE after SPH interpolation is solved by a preconditioned (diagonal scaling) Conjugate Gradient (PCG) method [31] with a convergence tolerance ($=1.0 \times 10^{-9}$).

In a similar way, the Laplacian operators for the temperature, concentration and nanoparticle volume fraction are given as

$$\langle \nabla^2 \theta(\boldsymbol{x}_i) \rangle = \sum_j m_j \left(\frac{\rho_i + \rho_j}{\rho_i \rho_j} \frac{\theta_{ij} R_{ij} \cdot \nabla W_{ij}}{R_{ij}^2 + \eta^2} \right), \tag{38}$$

$$\langle \nabla^2 \Phi(\boldsymbol{x}_i) \rangle = \sum_j m_j \left(\frac{\rho_i + \rho_j}{\rho_i \rho_j} \frac{\Phi_{ij} R_{ij} \cdot \nabla W_{ij}}{R_{ij}^2 + \eta^2} \right), \tag{39}$$

$$\langle \nabla^2 \varphi(\boldsymbol{x}_i) \rangle = \sum_j m_j \left(\frac{\rho_i + \rho_j}{\rho_i \rho_j} \frac{\varphi_{ij} R_{ij} \cdot \nabla W_{ij}}{R_{ij}^2 + \eta^2} \right), \tag{40}$$

Table 2 Effects of thermal Rayleigh number on *Nu* and *Sh* for different types of convection at $Ra = 10^4$, $Le = 1.0$, $Ln = 10$ and $Sr = 1.0$.

Case	*Ra*	*Nu*	*Sh*
Mono-diffusive regular fluid	10^3	0.9037	0.7033
	10^4	1.3461	0.8315
Mono-diffusive nanofluid	10^3	0.7459	0.8784
	10^4	1.1290	1.0364
Double-diffusive regular fluid	10^3	0.9160	0.6695
	10^4	1.3682	0.9558
Double-diffusive nanofluid	10^3	0.7089	0.8689
	10^4	1.1179	1.2128

5. Results and discussion

In this section, the obtained results were discussed. In fact, wide ranges for the governing parameters were considered, namely, thermal Rayleigh number ($10^3 \leqslant Ra_T \leqslant 10^4$), modified Dufour parameter ($0.03 \leqslant N_d \leqslant 0.6$) and Soret number ($0.1 \leqslant S_r \leqslant 2$). Also, four cases of convection were studied: Mono-diffusive regular fluid case ($Ra_{Tc} = 0$, $Nr = 0$) with ($Nb = 0$, $Nt = 0$, $Nd = 0$). Mono-diffusive nanofluid case ($Ra_{Tc} = 0$, $Nr = 0.2$), with ($Nb = 0.2$, $Nt = 0.2$, $Nd = 0$). Double-diffusive regular fluid case ($Ra_{Tc} = 0.2$, $Nr = 0$) with ($Nb = 0$, $Nt = 0$, $Nd = 0.2$). Double-diffusive nanofluid case ($Ra_{Tc} = 0.2$, $Nr = 0.2$) with ($Nb = 0.2$, $Nt = 0.2$, $Nd = 0.2$). It should be noted that the details of the calculations in the current study are clearly presented in Table 1. In all the obtained results, the value of Prandtl number was fixed at $Pr = 1.0$.

Firstly, the accuracy of the present results must be checked. This point can be observed from Figs. 3 and 4 which shows a comparison of compositional-dominated solution with Nishimura et al. [32] and Chamkha [33] for buoyancy ratio $N = 1.3$ and $N = 0.8$, respectively and $Le = 2.0$, $Pr = 1.0$, $Ra = 10^5$. It is found that, the present isothermal and isoconcentration contours and Nishimura et al. [32] and Chamkha [33] contours are almost similar. Therefore, we are confident that the results presented in this paper are very accurate.

Fig. 5 presents the isotherms, concentration and rescaled nanoparticle volume fraction lines and contours of horizontal and vertical velocities, respectively at $Ra = 10^4$, $Le = 1.0$, $Ln = 10$ and $Sr = 1.0$. It is observed that, in general, the isotherm lines gather beside the vertical walls, indicating thermal boundary layers beside the bottom of the left wall and top of the right wall of the enclosure. Regarding the solutal concentration lines, these contours are parallel to each other within the core of the cavity. Unlike the isotherms and isoconcentration contours, the nanoparticle volume fraction lines are distorted in the core. The contours of horizontal velocity component formed in the shape of two vertically-extended clockwise and anticlockwise circular cells next to the bottom and top walls of the enclosure. On the contrary, the contours

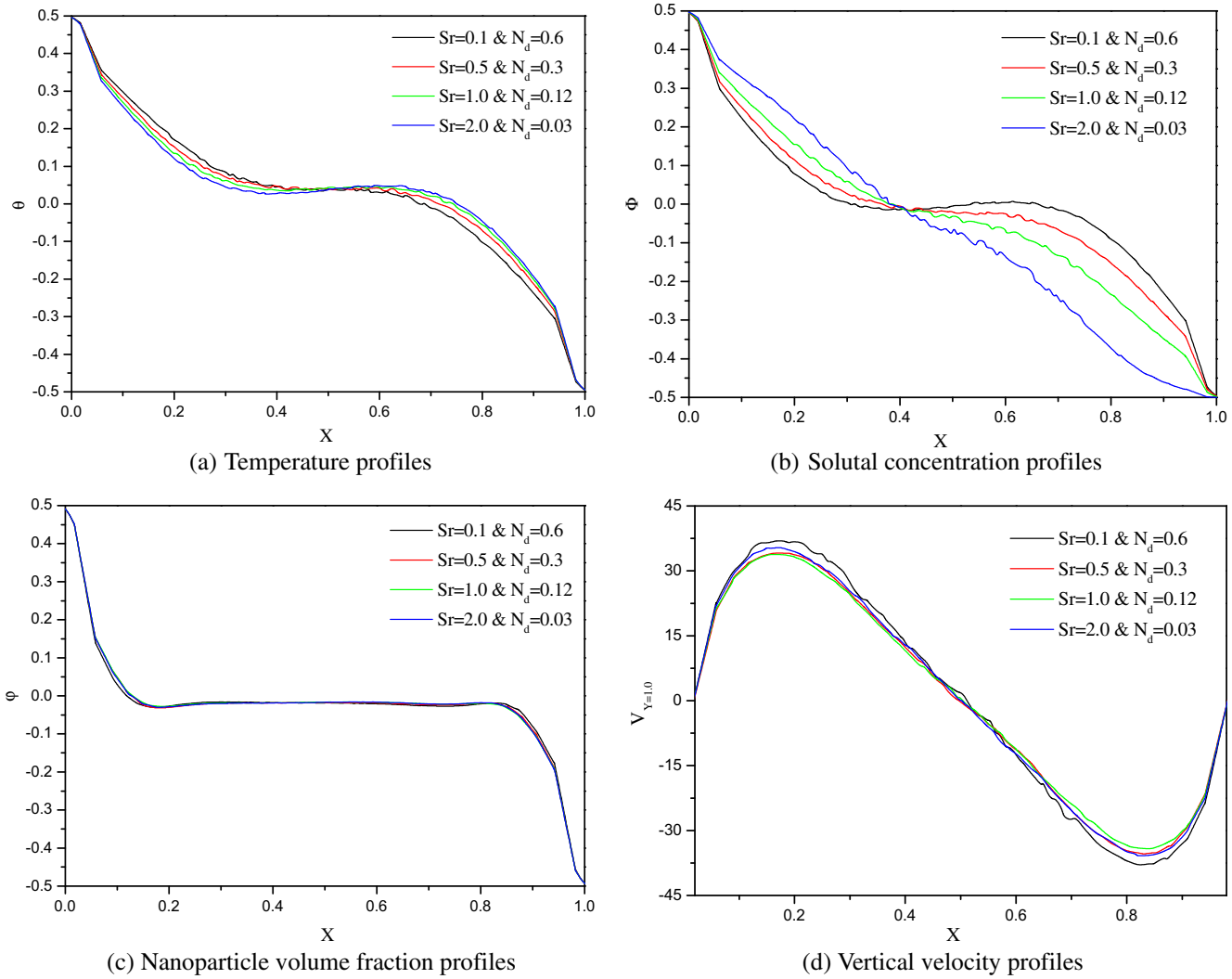

(a) Temperature profiles

(b) Solutal concentration profiles

(c) Nanoparticle volume fraction profiles

(d) Vertical velocity profiles

Figure 8 Effects of Soret and Dufour numbers on temperature, solutal concentration, nanoparticle volume fraction and vertical velocity profiles for the case of double-diffusive nanofluid at $Ra = 10^4$, $Le = 1.0$ and $Ln = 10$.

of the vertical velocity component formed in the shape of two horizontally-extended clockwise and anticlockwise circular cells next to left and right walls of the enclosure. Also, in view of Fig. 5a and b, we can observe a high natural convection can be obtained in case of double-diffusive than mono-diffusive. This can be noted from the following points: (a) the fluid flow is stronger in case of double-diffusive than mono-diffusive, (b) the distortion of nanoparticle volume fraction lines is more in case of double-diffusive than mono-diffusive. Adding the nanoparticle to the base fluid leads to shrinkage the thermal boundary layers mentioned previously and the distortion of the nanoparticle volume fraction lines does not occur in this case. However, the horizontal and vertical velocity components contours become more stretch in case of nanofluid than the case of the regular fluid.

Fig. 6 shows the temperature, solutal concentration, nanoparticle volume fraction, horizontal and vertical velocities, respectively for four cases, mono-diffusive regular fluid, mono-diffusive nanofluid, double-diffusive regular fluid and double-diffusive nanofluid at $Ra = 10^4$, $Le = 1.0$, $Ln = 10$ and $Sr = 1.0$. It is found that, at the end of the wall, the temperature takes its highest value in case of double diffusive nanofluid and takes its lowest value in case of mono diffusive regular fluid but we have the inverse of this behavior at the beginning of the wall. The Solutal concentration profiles differ in its behavior from the temperature, the double diffusive regular fluid gives a high concentration among all the cases and mono-diffusive nanofluid gives a lowest one. This behavior can be observed at the end of the wall; however, at the beginning of the wall, the mono diffusive regular fluid gives a high concentration and double diffusive nanofluid gives the lowest one. At the middle of the wall, the nanoparticle volume fraction profiles are not much affected by changing the convection mode from mono diffusive regular fluid to double diffusive regular fluid, whereas, it has a slightly decrease when the convection mode was switched off from regular fluid to nanofluid. Regarding the profiles of horizontal and vertical velocity components at the center line of the enclosure, the values of the velocities in case of double diffusive convection are higher than those of mono diffusive convection and this behavior is clearly evident at the bottom half of the enclosure but at the top half, the inverse behavior is observed. In any case, the presence of the nanoparticle in the base fluid supports the fluid flow.

Fig. 7 shows the snapshots of the temperature, solutal concentration, nanoparticle volume fraction, horizontal and vertical velocities, respectively at steady state for four cases, mono-diffusive regular fluid, mono-diffusive nanofluid, double-diffusive regular fluid and double-diffusive nanofluid at $Ra = 10^4$, $Le = 1.0$, $Ln = 10$ and $Sr = 1.0$. This figure confirms the observations that have been written previously. Table 2 displays the effects of thermal Rayleigh number on Nu and Sh for different types of convection at $Ra = 10^4$, $Le = 1.0$, $Ln = 10$ and $Sr = 1.0$. The results show that, the effect of nanofluid is a clear reduction in Nu and a clear enhancement in Sherwood number Sh and this effect for both mono diffusive and double diffusive. On the other hand, among all convection types under concentration, the rate of heat transfer gets its highest value in case of double diffusive regular fluid and the rate of mass transfer gets its highest value in case of double diffusive nanofluid. In any case, as usual in such kind of problems, an increase in thermal Rayleigh number leads to an increase in the temperature and concentration gradients and consequently increases both of average Nusselt number and average Sherwood number.

Table 3 Effects of Soret and Dufour numbers in Nusselt and Sherwood numbers for the case of double-diffusive nanofluid at $Ra = 10^4$, $Le = 1.0$ and $Ln = 10$.

Sr	Nd	Nu	Sh
0.1	0.6	0.9697	1.4262
0.5	0.3	1.0769	1.3256
1.0	0.12	1.1441	1.1753
2.0	0.03	1.1894	0.9153

Fig. 8 depicts the effects of Soret and Dufour numbers on temperature, solutal concentration, nanoparticle volume fraction and vertical velocity profiles for the case of double-diffusive nanofluid at $Ra = 10^4$, $Le = 1.0$ and $Ln = 10$. It is noted that, an increase in Sr accompanied by a decrease in Nd leads to increase both of fluid temperature and vertical velocity component in the left half of the enclosure. However, an inverse behavior is obtained for the fluid concentration. Table 3 displays the effects of Soret and Dufour numbers in Nusselt and Sherwood numbers for the case of double-diffusive nanofluid at $Ra = 10^4$, $Le = 1.0$ and $Ln = 10$. It is clear that, an increase in Sr accompanied by a decrease in Nd results in an increase in the gradient of the fluid temperature and a decrease in the concentration gradient which results in an enhancement in heat transfer rate and a reduction in the concentration transfer rate. In fact, to understand this effect, it is useful to give a definition for Dufour and Soret effects as the Dufour effect is the energy flux due to a mass concentration gradient occurring as a coupled effect of irreversible processes. It is the reciprocal phenomenon to the Soret effect.

6. Conclusion

In this study, the problem of double diffusive natural convection of a nanofluid in a rectangular enclosure was investigated. The governing equations were presented in a dimensional form and were converted to a dimensionless form using non-dimensional quantities. The incompressible smoothed particle hydrodynamic (ISPH) method was used to solve the dimensionless governing equations. Comparisons with previously published results were presented and found to be in a good agreement. The results of the current problem were presented for four cases, namely, mono diffusive regular fluid, mono diffusive nanofluid, double diffusive regular fluid and double diffusive nanofluid. From this investigation, we can conclude the following:

- The double diffusive mode gives a high natural convection in the enclosure.
- The presence of the nanoparticle in the base fluid leads to activity of the fluid motion.
- An increase in Soret number accompanied by a decrease in Dufour number results in an increase in average Nusselt number and a decrease in average Sherwood number.
- For both mono diffusive and double diffusive, a reduction in average Nusselt number and an enhancement in average Sherwood number can be obtained by considering nanofluid.

- An increase in thermal Rayleigh number leads to increase both of average Nusselt number and average Sherwood number.

References

[1] S.U.S. Choi, J.A. Eastman, Enhancing Thermal Conductivity of Fluids with Nanoparticles, 1995.

[2] H. Masuda, A. Ebata, K. Teramae, N. Hishinuma, Alteration of thermal conductivity and viscosity of liquid by dispersing ultra-fine particles, Netsu Bussei 7 (1993) 227–233.

[3] J. Buongiorno, W. Hu, Nanofluid coolants for advanced nuclear power plants, in: Proceedings of ICAPP '05, Seoul, 2005.

[4] S.K. Das, S.U.S. Choi, A review of heat transfer in nanofluids, in: F.I. Thomas, P.H. James (Eds.), Advances in Heat Transfer, Elsevier, 2009, pp. 81–197.

[5] S.K. Das, S.U.S. Choi, W. Yu, T. Pradeep, Nanofluids: Science and Technology, Wiley, Hoboken, NY, 2008.

[6] X.-Q. Wang, A.S. Mujumdar, Heat transfer characteristics of nanofluids: a review, Int. J. Therm. Sci. 46 (1) (2007) 1–19.

[7] M. Rahimi-Gorji, O. Pourmehran, M. Hatami, D.D. Ganji, Statistical optimization of microchannel heat sink (MCHS) geometry cooled by different nanofluids using RSM analysis, Eur. Phys. J. Plus 130 (2) (2015) 1–21.

[8] O. Pourmehran, M. Rahimi-Gorji, M. Hatami, S.A.R. Sahebi, G. Domairry, Numerical optimization of microchannel heat sink (MCHS) performance cooled by KKL based nanofluids in saturated porous medium, J. Taiwan Inst. Chem. Eng. 55 (2015) 49–68.

[9] M. Rahimi-Gorji, O. Pourmehran, M. Gorji-Bandpy, D.D. Ganji, An analytical investigation on unsteady motion of vertically falling spherical particles in non-Newtonian fluid by Collocation Method, Ain Shams Eng. J. 6 (2) (2015) 531–540.

[10] O. Pourmehran, M. Rahimi-Gorji, M. Gorji-Bandpy, D.D. Ganji, Analytical investigation of squeezing unsteady nanofluid flow between parallel plates by LSM and CM, Alexandria Eng. J. 54 (1) (2015) 17–26.

[11] C. Béghein, F. Haghighat, F. Allard, Numerical study of double-diffusive natural convection in a square cavity, Int. J. Heat Mass Transfer 35 (4) (1992) 833–846.

[12] S. Ostrach, Natural convection with combined driving forces, PCH/PhysicoChem. Hydrodyn. 1 (4) (1980) 233–247.

[13] J.W. Lee, Jae Min Hyun, Double-diffusive convection in a rectangle with opposing horizontal temperature and concentration gradients, Int. J. Heat Mass Transfer 33 (8) (1990) 1619–1632.

[14] Jae Min Hyun, J.W. Lee, Double-diffusive convection in a rectangle with cooperating horizontal gradients of temperature and concentration, Int. J. Heat Mass Transfer 33 (8) (1990) 1605–1617.

[15] M. Mamou, P. Vasseur, E. Bilgen, Analytical and numerical study of double diffusive convection in a vertical enclosure, Heat Mass Transfer 32 (1) (1996) 115–125.

[16] J.J. Monaghan, Simulating free surface flows with SPH, J. Comput. Phys. 110 (2) (1994) 399–406.

[17] J.P. Morris, P.J. Fox, Y. Zhu, Modeling low Reynolds number incompressible flows using SPH, J. Comput. Phys. 136 (1) (1997) 214–226.

[18] S.J. Cummins, M. Rudman, An SPH projection method, J. Comput. Phys. 152 (2) (1999) 584–607.

[19] M. Asai, A.M. Aly, Y. Sonoda, Y. Sakai, A stabilized incompressible SPH method by relaxing the density invariance condition, J. Appl. Math. 2012 (2012) 24.

[20] A.M. Aly, M. Asai, Y. Sonda, Modelling of surface tension force for free surface flows in ISPH method, Int. J. Numer. Methods Heat Fluid Flow 23 (3) (2013) 479–498.

[21] A.M. Aly, M. Asai, Y. Sonoda, Simulation of free falling rigid body into water by a stabilized incompressible SPH method, Ocean Syst. Eng., Int. J. 1 (3) (2011) 207–222.

[22] A.M. Aly, An Improved Incompressible Smoothed Particle Hydrodynamics to Simulate Fluid-Soil-Structure Interactions, Kyushu University, 2012 (Spheric home page).

[23] A.M. Aly, S.-W. Lee, Numerical simulations of impact flows with incompressible smoothed particle hydrodynamics, J. Mech. Sci. Technol. 28 (6) (2014) 2179–2188.

[24] A.K. Chaniotis, D. Poulikakos, P. Koumoutsakos, Remeshed smoothed particle hydrodynamics for the simulation of viscous and heat conducting flows, J. Comput. Phys. 182 (1) (2002) 67–90.

[25] K. Szewc, J. Pozorski, A. Tanière, Modeling of natural convection with smoothed particle hydrodynamics: non-Boussinesq formulation, Int. J. Heat Mass Transfer 54 (23–24) (2011) 4807–4816.

[26] M.E. Danis, M. Orhan, A. Ecder, ISPH modelling of transient natural convection, Int. J. Comput. Fluid Dyn. 27 (1) (2013) 15–31.

[27] A.M. Aly, Modeling of multi-phase flows and natural convection in a square cavity using an incompressible smoothed particle hydrodynamics, Int. J. Numer. Methods Heat Fluid Flow 25 (3) (2015) 513–533.

[28] A.M. Aly, M. Asai, Modelling of non-Darcy flows through porous media using extended incompressible smoothed particle hydrodynamics, Numer. Heat Transfer, Part B: Fundam. 67 (3) (2015) 255–279.

[29] A.M. Aly, S.E. Ahmed, An incompressible smoothed particle hydrodynamics method for natural/mixed convection in a non-Darcy anisotropic porous medium, Int. J. Heat Mass Transfer 77 (2014) 1155–1168.

[30] J. Buongiorno, Convective transport in nanofluids, J. Heat Transfer 128 (3) (2005) 240–250.

[31] J.A. Meijerink, H.A.v.d. Vorst, An iterative solution method for linear systems of which the coefficient matrix is a symmetric M-matrix, Math. Comput. 31 (137) (1977) 148–162.

[32] T. Nishimura, M. Wakamatsu, A.M. Morega, Oscillatory double-diffusive convection in a rectangular enclosure with combined horizontal temperature and concentration gradients, Int. J. Heat Mass Transfer 41 (11) (1998) 1601–1611.

[33] A.J. Chamkha, Double-diffusive convection in a porous enclosure with cooperating temperature and concentration gradients and heat generation or absorption effects, Numer. Heat Transfer, Part A: Appl. 41 (1) (2002) 65–87.